Contrib Mineral Petrol (1998) 130: 304–319 © Springer-Verlag 1998

Gordon Moore · I.S.E. Carmichael

The hydrous phase equilibria (to 3 kbar) of an andesite and basaltic andesite from western Mexico: constraints on water content and conditions of phenocryst growth

Received: 10 December 1996 / Accepted: 21 August 1997

Abstract We have conducted high pressure (to 3 kbar), water saturated melting experiments on an andesite (62 wt% SiO_2) and a basaltic andesite (55 wt% SiO_2) from western Mexico. A close comparison between the experimental phase assemblages and their compositions, and the phenocryst assemblages of the lavas, is found in water saturated liquids, suggesting that the CO_2 content was minimal in the fluid phase. Thus the historic lavas from Volcan Colima (with phenocrysts of orthopyroxene, augite, plagioclase, and hornblende) were stored at a temperature between 950–975 °C, at a pressure between 700–1500 bars, and with a water content of 3.0–5.0 wt%. A hornblende andesite (spessartite) from Mascota, of nearly identical composition but with only amphibole phenocrysts, had a similar temperature but equilibrated at a minimum of 2000 bars pressure with a dissolved water content of at least 5.5 wt% in the liquid. Experiments on the basaltic andesite show that the most common natural phenocryst assemblages (olivine, ±augite, ±plagioclase) could have precipitated at temperatures from 1000–1150 °C, in liquids with a wide range of dissolved water content (~2.0–6.0 wt%) and a corresponding pressure range. A lava of the same bulk composition with phenocrysts of hornblende, olivine, plagioclase, and augite is restricted to temperatures below 1000 °C and pressures below 2500 bars, corresponding to < 5.5 wt% water in the residual liquid. Although there is some evidence for mixing in the andesites (sporadic olivine phenocrysts), the broad theme of the history of both lava types is that the phenocryst assemblages for both the andesitic magmas and basaltic andesitic magmas are generated from degassing and reequilibration on ascent of initially hydrous parents containing greater than 6 wt% water. Indeed andesitic magmas could be related to a basaltic andesite parent by hornblende-plagioclase fractionation under the same hydrous conditions.

G. Moore (✉)[1] · I.S.E. Carmichael
Department of Geology and Geophysics,
University of California, Berkeley, CA 94720, USA

Present address:
[1]Department of Geology,
Arizona State University, TEmpe, AZ 85287-14-4, USA

Editorial responsibility: T.L. Grove

Introduction

Andesite lavas from the western Mexican volcanic belt contain a variety of phenocrysts ranging from only hornblende, to the most common, plagioclase-hornblende-2 pyroxene-titanomagnetite assemblages. This diversity of phenocryst suites, despite similarity in bulk composition, indicates different conditions of magma storage and phenocryst growth prior to eruption, and it is to quantify these conditions that this paper is concerned. Similarly, basaltic-andesite lavas have an array of phenocryst assemblages, typically without plagioclase, but their higher temperatures relative to andesites make hornblende phenocrysts rare among these lavas.

While we have known for some time the role that water plays in the generation of continental subduction-related magmatism relative to that in island arc settings (Osborn 1959; Ewart 1982; Merzbacher and Eggler 1984), the majority of hydrous phase equilibria studies on subduction-related lavas (e.g., andesites and basaltic andesites) have focused on the high pressure assemblages of these rocks (e.g., Baker and Eggler 1987; Eggler and Burnham 1973; Eggler 1972; Holloway and Burnham 1972) in order to test hypotheses of possible mantle sources (Osborn 1959; Green and Ringwood 1968). Fewer studies have been conducted concerning the upper crustal conditions (1–3 kilobars) at which most subduction-zone magmas appear to reside prior to eruption (Luhr 1990; Rutherford and Devine 1988; Rutherford et al. 1985; Merzbacher and Eggler 1984; Sisson and Grove 1993a, b). Small amounts of water dissolved in these magmas at crustal conditions can have significant effects on their phase assemblages, consequently influencing evolution of melt composition. For example, water contents greater than 2 wt% in basaltic

melts lowers the crystallization temperature and proportion of plagioclase, and changes its equilibrium composition, while at the same time stabilizing olivine (Sisson and Grove 1993a); as water changes the composition of the residual liquid, so will it change the fractionation path taken by the magma.

Due to the unique tectonic environment of the western Mexican volcanic belt (WMVB), the influence of water on subduction-related magmatism is extensively displayed. In addition to unusual hydrous, alkaline lava types (minettes, absarokites) not normally associated with subduction (Carmichael et al. 1996; Wallace and Carmichael 1992; Wallace et al. 1992), calc-alkaline lavas of nearly identical composition have widely different phenocryst assemblages. We have used this phenocryst diversity to constrain experimentally the storage conditions prior to eruption of magmas from the Mexican volcanic belt, and to quantify the water contents in the residual liquids required by their phenocryst assemblages.

For this experimental study, we have chosen two representative calc-alkaline lavas from western Mexico: a basaltic andesite and an andesite (Mas-22 and Mas-12 respectively; Table 1; described in Carmichael et al., 1996). Lavas with similar compositions are found throughout the entire Mexican volcanic belt (Fig. 1) and in continental volcanic arcs worldwide (Hasenaka and Carmichael 1987; Gill 1981). Lange and Carmichael (1990) noted the distinctive lack of plagioclase in basaltic andesites (52–55 wt% SiO_2) and the presence of Mg-rich ($Fo_{70–90}$) olivine both as phenocrysts and in the groundmass in many lavas from the San Sebastian area (Fig. 2), and Carmichael et al. (1996) described a hornblende lamprophyre of similar composition from the

Table 1 Wet chemical analyses of whole rock compositions and modal percent of phenocrysts in lavas. Wet chemical analyses for Mas-12, 22, 405 from Carmichael et al. (1996); Col-7 from Luhr and Carmichael (1980). Modal data for Col-7 from Luhr and Carmichael (1980), Mas-22, 12, 405 from Carmichael et al. (1996)

Composition	Spessartite (Mas-12)	Colima andesite (Col-7)	Hornblende lamprophyre (Mas-405)	Basaltic andesite (Mas-22)
SiO_2	62.64	61.61	55.25	55.25
TiO_2	0.63	0.60	0.83	0.74
Al_2O_3	17.25	17.82	17.32	17.41
Fe_2O_3	2.01	2.10	4.04	1.96
FeO	2.01	2.96	2.06	4.22
MgO	2.65	2.54	5.59	6.68
CaO	5.64	5.70	7.09	7.28
Na_2O	4.05	4.77	4.21	3.97
K_2O	1.61	1.43	2.06	1.18
P_2O_5	0.24	0.20	0.23	0.27
H_2O+	0.80	0.10	0.49	0.61
Total	99.53	99.73	99.28	99.57
Plagioclase	2.4	22.2	0.1	6.5
Orthopyroxene	–	2.9	–	–
Augite	–	1.8	1.6	2.6
Olivine	–	tr	1.1	6.5
Hornblende	3.8	1.5	5.6	–
Groundmass	76.0	61.3	84.5	72.0

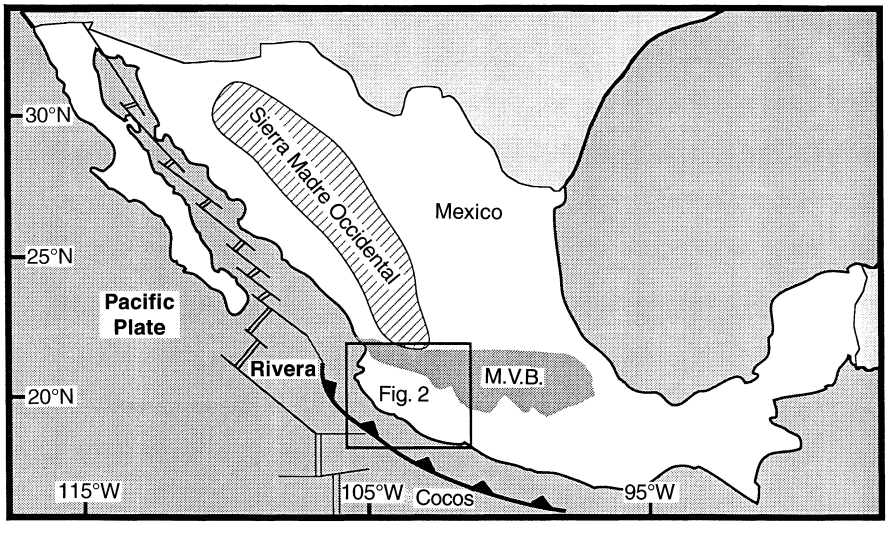

Fig. 1 General map of Mexico showing the oceanic plates, spreading centers, and the Middle American trench. *Box* is area of western Mexico shown in Fig. 2. *Lined area* is the Sierra Madre Occidental ashflow province; *shaded area* labeled *MVB* is the Mexican Volcanic belt

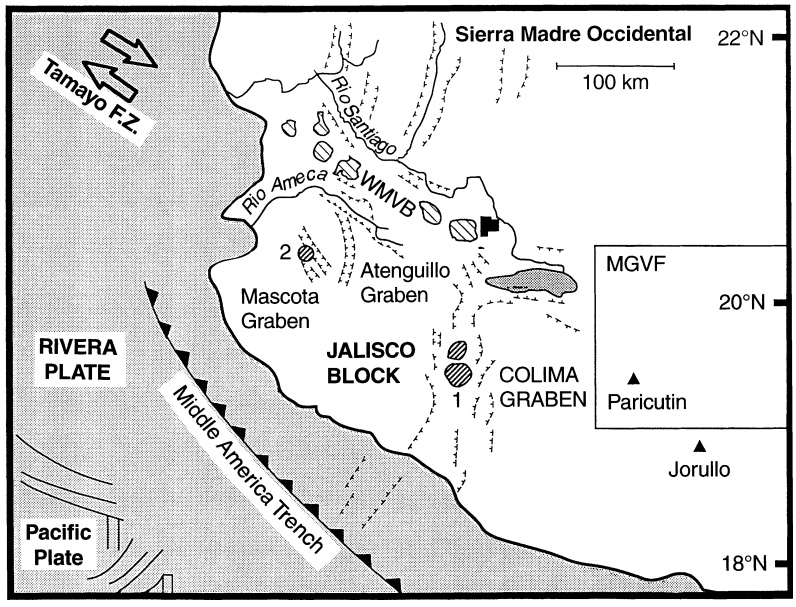

Fig. 2 Geologic map of the Jalisco Block, western Mexico, showing the major tectonic features. (*WMVB* the western Mexican volcanic belt, *MGVF* the Michoacan-Guanajuato volcanic field). The *numbers 1* and *2* respectively are the locations of Volcan Colima and the Mascota-San Sebastian volcanic field discussed in the text

Mascota region with phenocrysts of hornblende, olivine, augite and minor plagioclase. These assemblages contrast with the postulated low-water assemblages (orthopyroxene plus plagioclase) of the basaltic andesites from the Michoacan-Guanajuato volcanic field (MGVF in Fig. 2) in the central Mexican volcanic belt (Hasenaka and Carmichael 1987). Distinctive phenocryst assemblages in andesites are also thought to be related to preeruptive water contents. For example, the selected andesite sample (62 wt% SiO_2) was erupted as a spessartite (a confusing name, but a variety of lamprophyre) with only phenocrysts of hornblende (Table 1), near the town of Mascota (Fig. 2); in contrast, a nearly compositionally identical lava occurs as a lava flow at Volcan Colima (Fig. 2), with phenocrysts of plagioclase, augite, orthopyroxene, and hornblende (Table 1) (Luhr and Carmichael 1980) approximately 250 km to the SE of Mascota (Carmichael et al. 1996).

Given these observations of varying phenocryst assemblages in calc-alkaline lavas from the same volcanic arc, we have conducted melting experiments to quantify the equilibrium conditions and water contents associated with the phenocrysts of each lava type.

Experimental technique

One atmosphere experiments

The two samples (Mas-12 and Mas-22; Table 1) were equilibrated at one atmosphere pressure in a Deltech resistive furnace with CO/CO_2 gas mixtures controlling the oxygen fugacity at approximately the nickel-nickel oxide oxygen buffer (NNO). The gas flow rates were controlled using Linde Standard Response Flow Control Modules connected to a Linde Operator console, allowing total flow rates on the order of 100 cubic cm per minute. Oxygen fugacities were measured at the sample using a solid zirconia electrolyte oxygen sensor (SirO2 C700+) built by Ceramic Oxide Fabricators. The sensor was calibrated against the NNO buffer at 1100 °C and was found to be within ± 0.1 log units of the expected value of the oxygen fugacity (Huebner and Sato 1970). Temperature was measured using a "type S", Pt-PtRh10 thermocouple that also served as one of the leads for the zirconia oxygen sensor. The thermocouple was calibrated against the melting point of gold, and was found to be within $\pm 5°$ of the accepted value (1064 °C).

The experimental sample consisted of a paste of polyvinyl alcohol (PVA) and rock powder placed on a Pt loop, which was subsequently hung from a Pt wire cage and suspended in the furnace using a thin Pt quench wire. Quenching was accomplished by melting the quench wire and dropping the sample cage into a cup of distilled water placed at the bottom of the furnace. At no time did the samples leave the gas stream. All runs used Pt loops that were presaturated with iron to minimize iron loss. This was achieved by running the loop with sample for 24 hours at the oxygen fugacity and temperature of interest, quenching it and dissolving the glass off the loop by placing it in HF overnight. Fresh rock powder was then placed on the "iron saturated" loop, and run at the same conditions. The quenched products were then analyzed on the electron microprobe and the results are given in Table 2.

Experiments at elevated pressure

The hydrous experiments were conducted in an internally heated pressure vessel (IHPV) using the vertical "rapid quench" design described in Holloway et al. (1992). Pressure was measured with a calibrated Heise gauge accurate to ± 5 bars, while temperature was measured across the assembly using three sheathed "K" type thermocouples calibrated to ± 5 °C of the melting point of gold. Temperature gradients across the sample were controlled using a dual winding furnace connected to a variable transformer, and were never greater than 15 °C over the length of the sample capsule. Larger temperature differences often occurred however between the sample and oxygen sensor capsule (described below) depending on run conditions. Further modification of the furnace design during the course of the study eliminated any temperature gradient over the entire capsule assembly (5 cm). Previously, Holloway et al. (1992) reported unstable convection and thermal gradients in their vessel above 1.5 kilobars, but we were able successfully to conduct runs to the pressure limit of our vessel (3 kbar) without significant or unstable temperature gradients over ~5 cm length. Holloway et al.s furnace was approximately 20 cm long, and the sample tube is only half that, whereas our sample tube and furnace are 45 and 52 cm in length respectively. It is possible that the increased length

Table 2 Run conditions and phases for 1 atmosphere experiments (*Opx* orthopyroxene, *aug* augite, *plag* plagioclase) *ol* olivine)

Sample #	*T*- °C	Log f_{O_2}	Phase	SiO_2	TiO_2	Al_2O_3	FeO_2	MgO	CaO	Na_2O	K_2O	Total
Andesite:												
WD-5A	1251	−6.8	Gl									
WD-6A	1199	−8.1	Gl	63.4	0.64	16.1	4.54	2.8	5.16	3.0	1.75	97.4
			Plag	52.2	0.05	30.7	0.70	0.1	13.40	3.5	0.16	100.8
WD-7A	1099	−8.1	Gl	71.3	0.75	12.6	3.63	1.4	2.66	1.6	2.72	96.7
			Opx	55.8	0.38	3.1	11.88	25.2	1.53	0.1	0.30	98.4
			Aug	41.9	1.85	6.8	23.63	16.6	7.10	0.9	0.06	98.8
			Plag	52.8	0.07	29.1	0.82	0.1	12.11	4.2	0.23	99.4
			Oxide									
WD-8A	1149	−4	Gl	64.3	0.80	14.5	5.76	4.8	4.75	2.4	1.78	99.1
			Plag	52.2	0.03	31.2	0.77	0.1	13.43	3.6	0.17	101.3
			Oxide									
Basaltic andesite:												
WD-5B	1251	−6.8	Gl									
WD-6B	1199	−8.1	Gl	55.9	0.75	17.3	6.26	6.5	7.50	3.8	1.16	99.1
WD-7B	1099	−8.1	Gl									
			Plag	53.6	0.07	29.3	1.03	0.1	12.09	4.2	0.26	100.6
			Opx	54.7	0.34	1.2	15.43	25.9	2.41	0.1	0.07	100.1
			Ol	39.6	0.02	0.08	20.28	40.6	0.21	–	–	100.8
			Oxide									
WD-8B	1149	−8.4	Gl	59.7	1.03	15.6	6.68	4.5	6.34	3.4	1.73	99.0
			Plag	50.4	0.03	32.0	0.79	0.1	14.20	3.3	0.10	100.9
			Oxide									

stabilizes the convection within the sample tube to higher pressures, thereby allowing the rapid quench design to be used at pressures to 3 kilobars and possibly higher.

The pressure medium within the vessel consisted of H_2-Ar mixtures that also served to set the oxygen fugacity within the sample. All runs used a mixture of 0.10 vol.% H_2-99.90 vol.% Ar. This gas composition results in an effective oxygen fugacity within the pressure vessel of approximately one to two log units above the Ni-NiO buffer. It must be kept in mind that oxygen fugacity is not controlled by a solid assemblage oxygen buffer and varies with run temperature and vessel conditions, but is measured using a Ni-Pd alloy sensor in these experiments (described below). It was found that for runs of greater than or equal to 72 hours duration the sample appeared strongly oxidized, while the sensor gave oxygen fugacity values equivalent to air. This was most likely due to the continuous loss of hydrogen to the vessel walls, so for any run greater than 48 hours the H_2-Ar gas was replenished to maintain the oxygen fugacity at the ~NNO + 2 value (e.g., PEM12-22 with a 96 h run time). Another factor that affected the oxygen fugacity appeared to be the amount of time between runs. If several days elapsed with the vessel exposed to air, the first run following this period was always oxidized (e.g., PEM22-12 and PEM22-13). This is either due to oxidation of the vessel walls, or there is a curing process that occurs with the hydrogen diffusing into the steel during the run and then out again, with the outward diffusion having a timescale of days at room conditions. As the sensors from most of the 48 hour runs gave oxygen fugacity values close to that predicted from the composition of the gas mixture (NNO + 1), it is clear that the oxygen fugacity was not drifting significantly during the course of most of the experiments.

The sample assembly consisted of two capsules: a sample melt capsule and an oxygen sensor capsule. For experiments below 1150 °C Ag70Pd30 tubing (0.01'' wall thickness) was used, while runs greater than this temperature used Ag60Pd40. Both of these alloys are known to minimize, if not eliminate, iron loss from the sample (Sisson and Grove 1993a); under the experimental conditions reported here, the iron contents of the high temperature run capsules were always below detection with the electron microprobe (400 ppm). Vesiculation of the samples was not a problem, and whole rock powder (40–50 mg) for both compositions was used. The rock powder was placed into the sample capsule with a minimum amount of water added (~5–8 mg) to saturate the sample. The capsule was then welded, weighed, and dried for 30 minutes at 150 °C to check for leaks. The ambient oxygen fugacity of each experiment was measured using a sensor that consisted of a calibrated Ni-Pd alloy (Taylor et al. 1992; Pownceby and O'Neil 1994) that was loaded, along with a measured amount of water (~15–25 mg), into the second capsule of the assembly. The experimental details of our application of this sensor technique are given in Moore et al. (1995).

After running and quenching the samples as described above for a minimum of 48 hours, both capsules were weighed and punctured and then reweighed after heating in a drying oven at 150 °C for 10 minutes. Puncturing typically resulted in a loud hiss or a bead of water oozing out of the capsule. If the melt capsule did not lose weight after puncturing and heating, the run was discarded.

Microprobe analyses

Microprobe analyses were done on the ARL-SEMQ eight-channel electron microprobe or a Cameca SX-50 microprobe at UC Berkeley. All mineral phases were analyzed using an accelerating voltage of 15 kV, with a beam current of 30 nA measured on MgO, a 10 second counting time, and a focused beam with a 2 micron diameter. The reported compositions for all of the experimental phases are the average of at least 10 different point analyses taken across a representative phase. Hydrous glass analyses used a 20 micron beam and a 10 nA beam current that minimizes the typical decay of the alkalis that occurs in these glasses. The totals were calculated using the predicted water contents of Moore et al. (1998) and are adequate even up to 5 wt% dissolved water (Tables 3 and 4). The Ni-Pd alloy compositions of the oxygen sensors were analyzed using a focused beam and a sample current of 40 nA. The reported alloy compositions are the average of 5–10 individual grain analyses, between which the standard deviation was never larger than 3 mol% Ni.

Establishment of equilibrium

All runs were melting experiments and were held at the equilibrium temperature for a minimum of 48 hours. Several tests of equilib-

Table 3 Run conditions and phases for andesite composition high pressure experiments. X_{Ni} from electron microprobe analyses of Ni-Pd alloy sensor; Oxygen fugacity calculated from Pownceby and O'Neill (1994); (*Opx* orthopyroxene, *Aug* Augite, *Plag* plagioclase; *Hbde* hornblende, *Gl* glass, *Ox* oxide). Numbers in parentheses are the estimated modal% for the phases. ΔNNO calculated using Huebner and Sato (1970) FeOt total iron as FeO. See Table 6 for oxide compositions

Sample #	*P*-bars	*T*- °C	X_{Ni}	Logf_{O_2}	ΔNNO	Phase	SiO_2	TiO_2	Al_2O_3	FeOt	MgO	CaO	Na_2O	K_2O	H_2O	Total
PEM12-8	1985	1100	0.13	−6.1	+2.6	Gl									5.0	
PEM12-9	1527	1100	0.15	−6.3	+2.5	Gl									4.3	
PEM12-6	1065	1100	0.16	−6.4	+2.4	Gl									3.5	
PEM12-7	703	1100	0.32	−7.5	+1.3	Gl									2.8	
PEM12-15	483	1100	0.14	−6.2	+2.6	Gl	61.4	0.61	16.1	3.53	2.8	4.72	4.6	1.72	2.2	97.8
						Plag (7)	51.3	0.04	30.5	0.68	0.1	12.72	3.8	0.14		99.3
PEM12-2	1074	1075	0.16	−6.3	+2.8	Gl									3.5	
PEM12-14	1703	1050	0.16	−7.0	+2.4	Gl									4.7	
PEM12-13	1531	1050	0.33	−8.2	+1.2	Gl									4.4	
PEM12-1	1038	1050	0.16	−7.2	+2.2	Gl (99)	60.7	0.49	17.4	3.76	2.2	5.29	4.6	1.64	3.5	99.6
						Opx (1)	54.5	0.28	1.9	14.31	27.5	1.61	0.03	0.01	–	100.0
PEM12-21	2785	1030	0.22	−7.8	+1.9	Gl									6.3	
PEM12-17	1927	1025	–	–		Gl									5.2	
PEM12-3[a]	1051	1025	0.18	−7.3	+2.5	Gl										
						Opx	55.6	0.19	0.9	13.60	28.3	1.42	0.03	0.01	–	100.0
						Plag	51.9	0.09	30.3	0.73	0.2	13.22	3.6	0.14	–	100.2
PEM12-20	2834	1000	–	–		Gl									6.4	
PEM12-12	1475	1000	0.27	−8.6	+1.6	Gl (91)	60.4	0.58	15.8	3.62	2.0	4.95	3.9	1.83	4.4	97.6
						Opx (2)	54.4	0.23	2.1	14.38	27.1	1.27	0.02	0.01	–	99.5
						Plag(7)	51.8	0.14	29.5	1.33	0.5	13.32	2.8	0.32	–	99.7
PEM12-4	1055	1000	0.34	−7.4	+2.8	Gl (71)	63.4	0.68	16.2	3.03	1.5	3.62	3.6	2.01	3.7	97.7
						Opx (6)	55.8	0.20	0.8	14.64	27.7	1.39	0.01	0.01	–	100.6
						Plag (22)	52.6	0.06	30.5	0.67	0.1	12.70	4.1	0.13	–	100.9
						Ox (1)										
PEM12-11	441	1000	–	–		Gl (66)	68.2	1.03	13.7	3.16	1.2	3.20	4.2	2.6	2.3	99.6
						Opx (6)	54.1	0.25	2.4	14.20	28.0	1.28	0.02	0.01	–	100.3
						Plag (26)	51.4	0.03	30.7	0.65	0.1	13.12	3.8	0.13	–	99.9
						Ox (1)										
						Aug (1)	51.4	0.93	3.2	6.58	16.3	20.70	0.3	0.02	–	99.4
PEM12-23	2944	975	0.10	−7.7	+2.8	Gl									6.6	
PEM12-26	2461	975				Gl									6.0	
PEM12-18	1800	975	0.20	−8.3	+2.2	Gl (88)	60.9	0.67	16.5	3.68	1.9	4.66	5.2	1.78	5.1	100.2
						Opx (5)	53.5	0.21	3.0	14.52	28.0	1.19	0.01	0.01	–	100.4
						Plag (6)	51.3	0.09	30.4	1.22	0.4	14.25	2.3	0.24	–	100.2
						Hbde (1)	46.4	1.39	10.6	8.10	17.4	11.42	2.0	0.38	–	97.7

PEM12-19	1008	975	0.37	−9.5	+1.1	Gl (89)	61.8	0.61	16.5	3.77	1.7	4.91	3.5	1.87	3.6	98.3
						Opx (3)	53.0	0.22	2.7	14.37	28.0	1.32	0.03	0.02	–	99.6
						Plag (6)	50.9	0.01	31.4	0.65	–	13.41	3.9	0.13	–	100.5
						Aug (2)	52.2	0.42	2.6	6.71	17.3	20.35	0.3	0.03	–	99.9
PEM12-28[a]	2178	970		–		Gl										
						Hbde	45.6	1.32	10.3	7.88	17.3	11.32	2.1	0.39	–	96.2
PEM12-22	710	960	0.26	−9.2	+1.6	Gl (74)	64.0	0.74	15.0	3.49	1.6	3.87	4.0	2.07	3.0	97.8
						Opx (3)	54.2	0.17	1.4	15.95	27.2	1.04	–	0.02	–	100.0
						Plag (18)	53.3	0.05	29.6	0.92	0.1	11.63	4.6	0.21	–	100.1
						Aug (3)	48.9	1.05	3.9	12.00	15.1	17.7	0.4	0.13	–	99.2
						Ox (2)										
PEM12-16	1717	950	0.26	−9.1	+1.9	Gl (74)	63.3	0.37	15.3	2.20	1.0	3.07	4.4	2.32	5.1	97.1
						Plag (13)	51.6	0.04	30.4	0.69	0.1	12.60	4.2	0.15		99.7

Sample #	*P*-bars	*T*- °C	X_{Ni}	Logf_{O_2}	ΔNNO	Phase	SiO_2	TiO_2	Al_2O_3	FeOt	MgO	CaO	Na_2O	K_2O	H_2O	Total
						Ox (1)										
						Hbde (12)	45.5	2.11	10.3	10.54	16.0	11.24	1.9	0.38		98.0
PEM12-10	1455	950	0.25	−9.7	+1.3	Gl (75)	63.1	0.63	15.5	2.65	1.1	3.35	3.9	2.27	4.5	97.0
						Opx (3)	53.8	0.20	2.5	14.21	27.6	1.26	0.01	–	–	99.6
						Plag (15)	52.1	0.02	29.9	0.65	0.05	12.48	4.2	0.09	–	99.5
						Ox (1)										
						Aug (4)	51.7	1.08	2.7	6.18	16.6	19.90	0.8	–	–	99.0
						Hbde (2)	44.6	1.68	12.2	9.96	15.6	11.17	2.1	0.37	–	97.7
PEM1 2-5	1010	950	–	–	–	Gl (60)	68.2	0.47	14.0	2.14	0.7	2.45	3.1	2.74	3.7	97.6
						Opx (8)	55.0	0.18	0.9	15.1	26.7	1.35	0.03	0.02	–	99.3
						Plag (26)	52.4	0.05	30.3	0.72	0.1	12.64	4.3	0.16	–	100.7
						Ox (1)										
						Aug (4)	51.4	1.17	3.1	6.05	15.5	21.01	1.1	0.03	–	99.4
						Hbde (1)	44.9	1.67	12.0	9.31	16.0	11.26	2.1	0.39	–	97.6
PEM12-27	2482	935	–	–	–	Gl (85)	59.9	0.34	15.5	1.75	1.4	4.33	3.7	1.73	6.1	94.8
						Plag (6)	50.5	0.03	30.1	0.61	0.1	12.66	3.9	0.13	–	98.0
						Hbde (7)	45.4	1.49	10.2	7.62	17.1	11.24	2.1	0.40	–	95.6
						Ox (1)										
PEM12-24	2992	925	–	–	–	Gl	55.9	0.53	15.2	3.13	1.7	4.75	3.5	1.56	6.7	93.0
						Hbde										
PEM12-25	2851	900	–	–	–	Gl (89)	58.7	0.51	15.5	3.01	1.6	4.48	3.5	1.63	6.6	95.5
						Plag (4)	48.3	0.10	32.2	0.57	0.1	15.11	2.7	0.08	–	99.2
						Hbde (6)	44.9	1.55	10.9	8.70	16.6	11.18	2.1	0.40	–	96.4
						Ox (1)										

[a]Slow quench with quench crystals found in glass
[b]wt% H_2O calculated from Moore et al. (1998) using glass probe analyses

Table 4 Run conditions and phases for basaltic andesite high pressure experiments. X_{Ni} from electron microprobe analyses of Ni-Pd alloy sensor; oxygen fugacity calculated from Pownceby et al. (1994); (phase abbreviations as in Table 3, and *ol* olivine). Numbers in parentheses are estimated modal% of phases. (*FeOt* total iron as FeO). △NNO calculated from Huebner and Sato (1970)

Sample #	*P*-bars	*T*- °C	X_{Ni}	Log f_{O_2}	ΔNNO	Phase	SiO_2	TiO_2	Al_2O_3	FeOt	MgO	CaO	Na_2O	K_2O	H_2O[b]	Total
PEM22-3	1103	1150	0.14	−5.7	+2.4	Gl	54.5	0.66	17.5	6.16	5.9	7.11	3.8	1.16	3.5	100.3
						Ox										
PEM22-7	731	1150	0.21	−5.9	+2.2	Gl (96)	53.9	0.68	18.4	5.56	5.5	6.44	4.7	1.24	2.8	99.2
						Ol (3)	41.2	0.03	0.03	11.13	48.5	0.11	–	0.02	–	101.0
						Ox (1)										
PEM22-5[a]	769	1125	0.18	−6.4	+2.0	Gl										
						Ol	40.4	0.01	0.01	10.75	48.0	0.19	–	0.02	–	99.4
PEM22-9	517	1125	0.18	−6.4	+2.1	Gl (90)	54.3	0.50	18.9	5.37	3.8	7.28	5.0	1.27	2.3	98.7
						Ol (7)	40.1	0.03	–	13.63	45.9	0.16	–	0.01	–	99.8
						Ox (1)										
						Plag (2)	50.2	0.06	31.4	0.75	–	14.05	3.42	0.11	–	100.0
PEM22-10	1572	1120	0.21	−5.7	+2.8	Gl	51.1	0.63	18.4	5.57	5.9	7.17	3.9	1.13	4.3	98.1
						Ox										
SAT-M22-2	1255	1100	–	–	–	Gl (97)	52.9	0.63	17.8	5.47	5.4	7.12	3.2	1.32	3.8	97.6
						Ol (3)	40.9	0.03	–	10.69	49.5	0.15	–	–	–	101.3
PEM22-2	1072	1100	0.16	−6.2	+2.6	Gl (96)	54.8	0.80	18.2	5.26	5.5	7.12	4.5	1.24	3.5	100.9
						Ol (3)	40.4	0.02	0.02	11.02	48.5	0.13	–	0.01	–	100.1
						Ox[c] (2)										
PEM22-13[a]	2102	1075	0.03	−4.9	+4.2	Gl										
						Ox										
PEM22-4[a]	1055	1075	0.13	−6.2	+2.9	Gl										
						Ol	40.6	0.01	0.03	11.16	47.7	0.17	–	0.01	–	99.7
						Ox										
PEM22-8	1017	1075	0.28	−7.1	+2.0	Gl (94)	51.6	0.76	18.8	5.93	4.5	7.79	4.4	1.21	3.4	98.4
						Ol (5)	40.0	0.02	0.03	13.02	45.7	0.18	–	0.02	–	99.0
						Ox (1)										
PEM22-6	607	1075	0.17	−6.4	+2.7	Gl (52)	58.5	0.91	16.9	5.03	2.8	5.35	2.2	1.74	2.5	95.9
						Ol (10)	39.9	0.02	0.02	15.29	44.1	0.20	–	0.02	–	99.6
						2 Ox (2)										
						Plag (30)	51.4	0.09	29.9	0.87	0.1	13.04	3.89	0.15	–	99.4
						Aug (6)	52.4	0.37	2.29	6.27	16.5	20.97	0.3	0.03	–	99.1
PEM22-12	2082	1050	0.01	−3.8	+5.6	Gl (96)	51.8	0.63	17.5	4.46	5.2	6.40	3.1	1.30	5.1	95.5
						Ol (3)	41.5	0.02	0.11	3.74	53.9	0.19	–	0.02	–	99.5
						Ox (1)										
PEM22-1	989	1050	0.20	−7.8	+1.6	Gl (71)	56.1	0.88	17.0	5.04	3.1	5.4	5.1	1.81	3.5	97.9
						Ol (8)	39.5	0.02	0.03	16.3	45.7	0.12	–	0.01	–	101.5
						Plag (14)	51.0	0.05	31.0	0.85	0.1	14.04	3.51	0.10	–	100.7
						Aug (6)	50.6	0.89	5.11	7.52	15.1	21.42	0.3	0.02	–	101.0
PEM22-18	2040	1025	–	–	–	Gl (86)	53.2	1.00	17.6	4.87	3.3	6.52	3.9	1.24	5.1	96.5
						Ol (8)	40.1	0.04	0.8	15.55	42.4	0.35	0.1	0.04	–	99.4
						Plag (3)	47.2	0.11	32.6	0.80	0.2	16.39	2.1	0.08	–	99.5
						Aug (3)	50.5	0.71	4.2	6.08	15.4	22.00	0.3	–	–	99.2
PEM22-19	3027	1000	–	–	–	Gl (82)	53.0	0.51	16.7	4.84	3.4	5.16	3.8	1.29	6.4	95.0
						Ol (2)	39.4	0.02	0.01	15.76	43.8	–	–	0.01	–	99.3
						Hbd (16)	42.9	1.51	12.2	9.05	16.2	10.97	2.42	0.41	–	95.7
PEM22-14[a]	2882	1000	–	–	–	Gl										
						Ol	40.5	0.02	0.02	11.54	47.4	0.15	–	–	–	99.2
						Plag										

				Aug	52.7	0.36	2.5	5.1	17.2	21.79	0.3	–	100.0
				Ox									
PEM22-20	2496	1000	–	–	Gl (76)	52.2	0.49	16.7	4.95	3.4	6.57	3.9	1.19	5.8	95.3
					Ol (3)	39.6	0.02	0.01	14.71	44.8	0.14	0.01	–	–	99.6
					Hbd (17)	42.8	1.74	11.9	8.88	16.4	11.12	2.44	0.40	–	95.8
					Aug (4)	50.2	0.75	4.37	6.97	14.8	21.7	0.35	0.01	–	99.4
PEM22-17	1613	1000	–	–	Gl (75)	55.7	0.82	17.4	3.3	3.1	5.64	4.2	1.47	4.6	96.2
					Ol (6)	40.8	0.02	–	9.36	49.2	0.12	–	–	–	99.5
					Plag (8)	48.6	0.02	31.6	0.76	0.1	15.2	2.8	0.08	–	99.2
					Aug (6)	50.1	0.79	4.2	6.94	15.4	21.52	0.4	0.02	–	99.4
					Ox (5)										
PEM22-16	2220	975	–	–	Gl (66)	56.2	0.33	17.4	2.93	2.2	5.00	3.1	1.44	5.3	93.9
					Hbd (28)	42.9	1.57	11.9	7.72	17.3	11.50	2.3	0.31	–	95.5
					Plag (3)	46.9	0.03	32.1	0.97	0.1	16.30	1.9	0.08	–	98.4
					Ox (2)										
PEM22-15	2806	950	–	–	Gl (65)	56.8	0.32	17.7	3.01	2.4	5.32	3.3	1.41	6.0	96.3
					Hbd (31)	43.4	1.59	12.3	9.39	16.2	10.99	2.4	0.37	–	96.8
					Plag (3)	46.9	0.01	33.2	0.79	0.1	16.7	1.9	0.05	–	99.7
					Ox (1)										

[a] Slow quench with quench crystals found in glass
[b] Wt% H_2O calculated from Moore et al. (1995)
[c] See Table 6 for oxide analyses

rium were conducted, including comparisons of runs with significantly longer run times. All phases in both the hydrous basaltic andesite and andesite runs were relatively homogeneous in composition and had euhedral shapes. For instance plagioclase, a typically slow mineral to equilibrate, only varied a maximum of 2 mol% in the An component from core to rim in the lowest temperature runs. Hornblende consistently showed some heterogeneity however in its Al and Ti content of up to several weight percent. For the andesite composition one of the lowest temperature experiments (PEM12-22) was run for 96 hours, with replenishment of the hydrogen-argon gas halfway through the experiment. This run showed no differences in zoning, homogeneity, or phenocryst morphology in any of the phases to indicate that it was significantly different from the 48 hour runs, suggesting that the 48 hour run time was sufficient for all phases to approach equilibrium closely. Also, the samples that were chosen as starting compositions had very low phenocryst contents (~8 and ~16% for Mas-12 and Mas-22 respectively; Table 1) with a fine-grained groundmass, with the benefit that relict crystals in the run products were not detected.

Results

The stability of the phenocryst minerals varies systematically in both the andesite and basaltic andesite as a function of water pressure and temperature (Figs. 3 and 4). Pressure-temperature phase diagrams constructed from the results of the experiments were also contoured with isopleths of dissolved water content using analyzed glass compositions and the water solubility expression of

Fig. 3 Water saturated pressure-temperature phase diagram for the andesitic composition (Mas-12). *Closed circles* are conditions for individual experiments. *Phase boundary lines* are phase-in lines plus liquid. *Sub-horizontal dashed lines* are isopleths of water concentration calculated from the residual glass compositions and the water solubility model of Moore et al. (1998). *Small numbers next to data points* in the plagioclase field give the anorthite content of the feldspars. *Box* represents the range of temperatures from pyroxene geothermometry for Colima lavas (Luhr 1990). (*Hbde* hornblende, *Opx* orthopyroxene, *Plag* plagioclase, *Aug* augite). Note the *shaded area* represents the conditions of equilibrium for the Colima assemblage and the *lined area* that for the Mascota spessartite

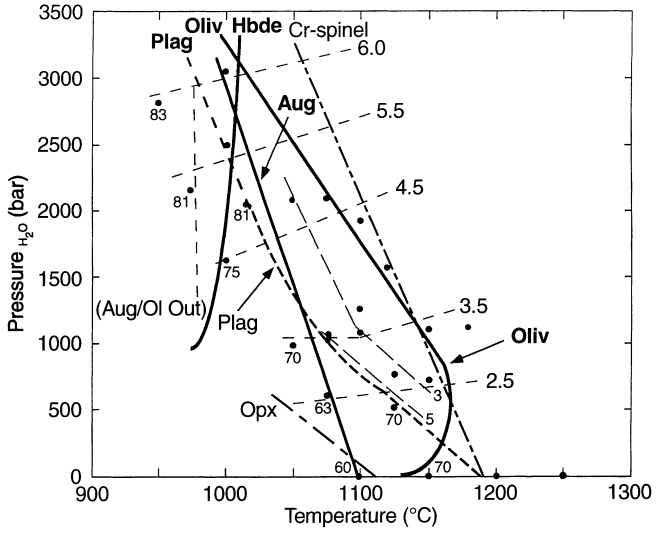

Fig. 4 Water saturated pressure-temperature phase diagram for the basaltic andesite composition (Mas-22). Abbreviations and symbols as in Fig. 4 (*Oliv* olivine). *Long dashed lines* in the olivine-only field are contours of estimated modal% olivine

Moore et al. (1998). With these diagrams it is easy to assess the water contents and pressure-temperature conditions necessary to stabilize the various natural phenocryst assemblages of andesites and basaltic andesites from the WMVB.

In order further to evaluate the relevance of the experimental conditions to the WMVB lavas, natural and experimental phase compositions and abundances were also compared. The modal abundance for each phase in the run products was calculated using a linear least squares mass balance analysis program (XLFRAC; Nicholls and Stormer 1978) and are given as the numbers in parentheses after the phases in Tables 3 and 4. This method is dependent on the precise analysis of all phases present, but as the measurement of the composition of the hydrous glass is subject to significant error on the electron microprobe, the calculated modes are commonly inexact. Relatively large residuals (>1.0) were encountered in several of the calculations for the silica and sodium components, particularly for the basaltic andesite composition, and are consistent with the recognized difficulty in the analysis of these elements. The majority of the calculations however, had a sum of the squares of the residuals for the entire calculation that was less than 2.0, indicating that the fits are reasonable.

Phase diagram and phase compositions and modes for andesite

All historical lava flows at Volcan Colima up to 1975 have phenocrysts of plagioclase (20–30 vol.%), orthopyroxene (1–4 vol.%), clinopyroxene (1–3 vol.%), hornblende (1–5 vol.%); and of these only the 1913 and 1961 eruptions are not similar in composition to the andesite used in this study (Table 1) (Luhr and Carmichael 1980). This particular assemblage is shown by the shaded area in Fig. 3. From the water isopleths (Fig. 3), we infer that the Colima magmas had between 3 and 5 wt% dissolved water, and resided at pressures between ~700–1700 bars at approximately 950–975 °C prior to eruption. The modal calculations for the experiments also show that there is approximately 60 wt% residual liquid (glass) at these conditions (Fig. 5; Table 3). All of these observations are in agreement with the range of water estimates for the 1961–1991 flows at Volcan Colima (2.5–3.5 wt% H_2O) based on plagioclase-melt equilibria (Luhr 1992), the pyroxene thermometry estimate (960–980 °C), and the modes of the natural phenocryst assemblages (Luhr and Carmichael 1980).

This agreement between the experiments and the observed characteristics of the lavas suggests that not only do the pressure and temperature conditions of the

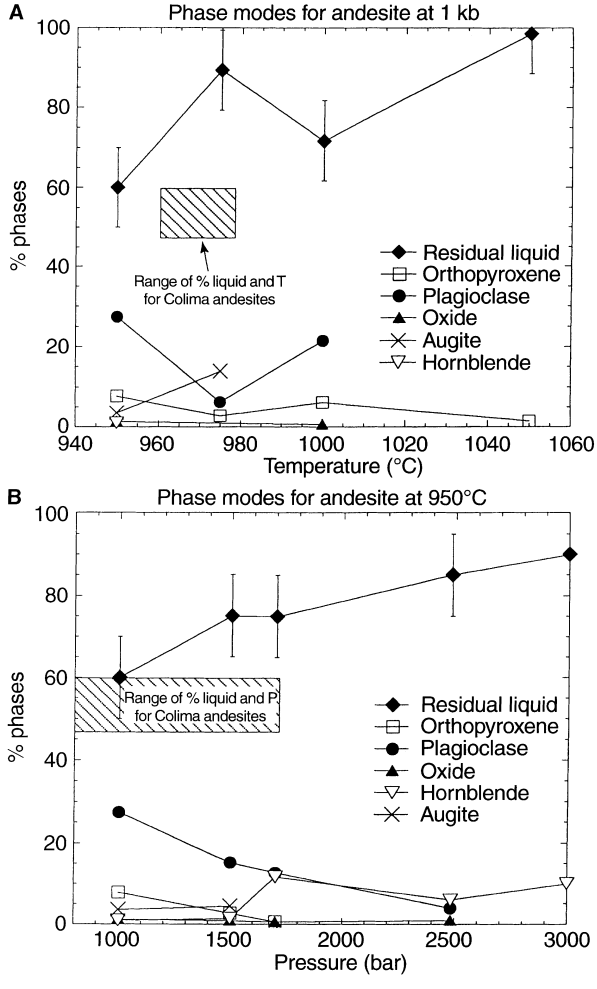

Fig. 5 A Phase modes as a function of temperature for the andesite composition at 1 kilobar pressure. The *lined box* represents the range of % groundmass and temperature estimated for the Colima andesites (Luhr and Carmichael 1980; Luhr 1990). *Error bars* on liquid estimated from largest calculated residuals. **B** Phase modes as a function of pressure for the andesite composition at 950 °C. *Lined box* represents range of % groundmass for the Colima lavas, as well as range of pressure for which the lava assemblage is stable at 950 °C.

experiments duplicate those of the magma, but also indicate that the Colima andesites were in equilibrium with a water-rich fluid phase that did not contain significant amounts of carbon dioxide. Eggler and Burnham (1973) showed that the stability of hornblende in an andesitic melt was not dramatically affected by the addition of up to $\sim$ 66 mol% CO_2 to the fluid. While this observation allows for the presence of significant CO_2, it is countered by the dependence of plagioclase composition on temperature and water fugacity (Housh and Luhr 1991), and also the effect of water fugacity on the modal amounts of the phenocrysts present, especially plagioclase (Fig. 5). For example, at 970 °C and 1800 bars (the upper stability limit for the Colima lavas), addition of $\sim$60 mol% CO_2 (assuming ideal mixing), would lower the water fugacity to $\sim$720 bars, which would increase the modal abundance of plagioclase well beyond the 30 modal percent maximum observed in the Colima andesites (Fig. 5). Several lines of evidence indicate that the fluid phase of the Colima lavas did not contain significant amounts of carbon dioxide.

1. The agreement between the experimental (water saturated) phase assemblage and phase abundance and the observed phenocryst data, at the temparatures of pyroxene phenocryst thermometry.
2. The correspondence between the plagioclase-melt water estimates and the calculated water solubility in the residual liquids (glasses) using the model of Moore et al. (1998)
3. The correspondence of the experimental phase compositions with those of the phenocrysts (see below).

For the Mascota spessartite phase assemblage of hornblende only (lined area, Fig. 3) we see that a *minimum* estimate of the preeruptive water content is 5.5 wt%, and that a pressure of approximately 2000 bars and a similar temperature to the Colima andesites is required to stabilize the hornblende-only assemblage. The upper bound on the pressure and water content of this assemblage is not constrained by our experiments and could be greater than 7 wt% H_2O (or 3 kbar). Note also in Fig. 3 the characteristic suppression of plagioclase with increasing P_{H_2O} from being the liquidus phase at 500 bars and 1100 °C, to being the third phase in (with Fe-Ti oxide) at 3000 bars and 925 °C. Hornblende is stabilized at higher pressures at the expense of orthopyroxene and plagioclase (Fig. 5), consistent with the work of Eggler (1972) and Eggler and Burnham (1973). In fact, orthopyroxene is not found in the presence of hornblende above 2000 bars of water pressure (dashed line for the orthopyroxene boundary, Fig. 3).

The estimated water content for the Mascota spessartite, in contrast to the Colima andesites, shows that pre-eruptive melt water contents may vary by as much as a factor of two in *magmas* of similar composition within the same volcanic arc. The amount of water that was necessary to stabilize this spessartite is impressive when it is considered that the magma was erupted as a flow, travelling up a longer ascent path (Carmichael et al. 1996), and that similar water contents are estimated for the spectacular explosive eruption in 1974 of Volcan Fuego in Guatemala (Sisson and Layne 1993). Another enigma presented by this particular flow is that the time elapsed between emplacement of the flow and degassing of its water had to be small, as the hornblendes show only slight reaction rims (Rutherford and Hill 1993) and are known to not be fluorine-rich amphiboles (Carmichael et al. 1996).

Phase compositions for the Colima phenocryst assemblage

As was discussed previously, the preeruptive temperature and water content for the Colima andesite assemblage have been constrained from both pyroxene thermometry and feldspar equilibria of the lavas (Luhr and Carmichael 1980; Luhr 1992). Comparison of the phase compositions from the experimental products and the phenocryst assemblage can be used further to refine estimates of the equilibrium pressure and eruption history.

The majority of phases produced in our andesitic experiments match in composition those found in the lavas (Table 5). Luhr and Carmichael (1980) report trace amounts of olivine however in their modal analysis, but no olivine compositions are given for samples similar to the one studied here, and no olivine was found in any of the experimental products; perhaps this is telltale evidence for magma mixing. The oxides in the experiments are titano-magnetite (Table 6), as are those found in the lavas (Luhr and Carmichael 1980). The similar Fe-Mg phase compositions (augite and opx) verify that the experiments were conducted at a similar oxygen fugacity (NNO + 2) to that of the natural system.

The other phenocryst phase, plagioclase, gives additional information on the crystallization history of the Colima lavas. For example, the modal abundance of plagioclase is equivalent in both the experiments and the lava (26% in the experiments and 20–30% in the lavas) suggesting a direct crystallization history for the magma (i.e., no magma mixing), yet there is some disparity in the more sodic rims of the phenocrysts (An_{46-52}) compared to the equilibrium crystals (An_{63} at 950 °C) in the run products. The experimental plagioclase compositions do fall within the range of the most calcic plagioclases (An_{58-85}) analyzed in the lavas by Luhr and Carmichael (1980), and it should be noted that An_{62} is the most common calcic plagioclase composition found in the Colima lavas, although no distinction is made between phenocrysts and microphenocrysts. As Housh and Luhr (1991) have shown that increasing melt water content stabilizes the $CaAl_2Si_2O_8$ component in plagioclase, the disparity between the calcic plagioclase phenocrysts and the experimental feldspars could be explained by a period of crystallization at higher water pressure (>2 kbar; Fig. 3) which gave rise to the more anorthite-rich feldspars. Following this period of crys-

Table 5 Comparisons of the composition ranges of phases for experimental and natural assemblages. Data for Colima from Luhr and Carmichael (1980); data for San Sebastian from Lange and Carmichael (1990)

Sample #	Orthopyroxene			Augite			Olivine		Plagioclase (calcic)			Hornblende[b]		
	X_{WO}	X_{EN}	X_{FS}	X_{WO}	X_{EN}	X_{FS}	X_{Fo}	X_{Fa}	X_{An}	X_{Ab}	X_{Or}	X_{MgO}	X_{FeOt}	X_{MgO}/X_{FeOt}
Andesite: Colima assemblage	0.02	0.70–0.72	0.25–0.28	0.40–0.42	0.43–0.48	0.10–0.15	–	–	0.58–0.85	0.15–0.42	0.01	0.19–0.24	0.07–0.10	2.1–3.4
Experimental Basaltic andesite:	0.02–0.03	0.73–0.76	0.21–0.24	0.31–0.40	0.44–0.48	0.10–0.20	–	–	0.59–0.77	0.41–0.23	0.01	0.22–0.24	0.06–0.08	2.7–4.0
San Sebastian suite	–	–	–	0.40–0.43	0.40–0.47	0.09–0.12	0.81–0.90 (cores)	0.10–0.18 (cores)	0.62–0.74	0.38–0.26	0.01	0.22	0.08	2.75
Experimental	–	–	–	0.38–0.40	0.43–0.48	0.10–0.12	0.83–0.89[a]	0.11–0.17[a]	0.60–0.83	0.40–0.17	0.01	0.23–0.25	0.06–0.08	2.9–4.2

[a] Excludes PEM22-12 due to oxidizing conditions
[b] Includes the spessartite Mas-12 with the andesite group and the hornblende lamprophyre Mas-405 with the basaltic andesite group from Carmichael et al. (1996)

tallization, simultaneous crystallization of plagioclase and degassing of water occurred during the ascent of the magma through the conduit, creating the albite-rich rims. This scenario is supported by the observation that the most sodium-rich feldspar cores found in the lavas are within 5 mol% Ab of their average rim composition, with 2 exceptions (Col-7 and Col-18, both with a difference of ~10 mol% Ab), as well as the presence of significant breakdown rims on the amphibole phenocrysts. Therefore we propose that the Na-rich feldspars found in the Colima lavas nucleated and grew during ascent, while the calcic plagioclase phenocrysts nucleated at higher pressures and grew Na-rich rims during ascent.

Phase compositions for the Mascota spessartite

Hornblende is the only phenocryst phase in the spessartite of Mascota, with plagioclase being a sporadic microphenocryst, so that constraints on the intensive variables are few. Because of the shape of the phase boundaries (Fig. 3), we are able to limit the preeruptive conditions and minimum water content to 950–975 °C and >2 kbar or ~5.5 wt% H_2O dissolved in the melt. The microphenocryst feldspar composition of An_{65} (Carmichael et al. 1996) observed in the spessartite is consistent with the composition of equilibrium feldspar generated in an experiment at 2.5 kbar and 935 °C (PEM12-27; Fig. 3), suggesting that the feldspar nucleated on ascent of the magma or that the magma had cooled below the plagioclase saturation temperature just prior to eruption. The lack of other phenocryst phases in the lava favors the latter scenario, as nucleation of feldspar only during decompression from the spessartite field is impossible given the geometry of the phase boundaries (Fig 3). The pristine nature of the hornblende phenocrysts in this lava also requires a rapid ascent (Rutherford and Hill 1993), making crystallization of other phases during ascent less likely.

The Fe/Mg ratio of the hornblende in the experiments appears to depend on oxygen fugacity, similar to the behavior of the other Fe-Mg phases, but does not appear to depend on pressure or temperature. The fact that the composition of the spessartite hornblende phenocrysts (MgO = 16.3 wt% for the core) (Carmichael et al. 1996) is slightly more magnesian than that found in the Colima assemblage (wt% MgO = 14.5–15.5, Col-7) (Luhr and Carmichael 1980) suggests that the spessartite equilibrated at a higher oxygen fugacity than that found at Colima. The calculated values of oxygen fugacity, using the measured ferric-ferrous ratios of the bulk rocks (Table 1), the empirical calibration of Kress and Carmichael (1991), and a temperature of 950 °C for both assemblages, are consistent with this inference ($\log f_{O_2} = -8.3$ and -9.1; for Mas-12 and the Colima andesite Col-7 respectively).

Table 6 Representative oxide compositions for andesite and basaltic andesite experiments (FeOt total iron as FeO)

Sample #	*P*-bars	*T*-°C	Logf_{O2}	SiO_2	TiO_2	Al_2O_3	FeOt	MgO	MnO	CaO	Cr_2O_3	V_2O_3	NiO	Total
Andesite:														
PEM12-4	1055	1000	−7.4	0.2	4.14	3.5	80.29	4.5	0.26	0.28	0.02	0.15	0.23	93.5
PEM12-5	1010	950	−9.3	0.2	12.01	1.9	74.61	3.1	0.25	0.13	0.02	0.35	0.09	92.7
PEM12-10	1455	950	−9.7	0.4	6.60	3.3	78.00	3.66	0.27	0.11	0.02	0.33	0.14	92.8
PEM12-11	441	1000	−8.4	0.1	4.77	3.2	80.74	4.3	0.29	0.10	0.08	0.24	0.34	94.2
PEM12-16	1717	950	−9.1	0.1	8.4	2.7	77.47	3.2	0.31	0.11	0.03	0.24	0.07	92.7
PEM12-22	710	960	−9.2	0.7	4.82	3.6	77.89	4.2	0.25	0.17	0.07	0.22	0.38	92.3
Basaltic andesite:														
PEM22-2	1072	1100	−6.2	0.1	0.67	20.0	24.54	14.1	0.24	0.18	39.01	0.20	0.18	99.2
PEM22-3	1103	1150	−5.7	0.2	0.42	13.2	30.73	13.7	0.21	0.23	37.30	0.11	0.38	96.4
PEM22-4	1055	1075	−6.2	0.1	0.49	14.3	31.02	11.9	0.30	0.19	38.95	0.12	0.18	97.6
PEM22-5	769	1125	−6.4	0.5	0.66	13.7	36.97	12.0	0.29	0.39	30.76	0.13	0.23	95.7
PEM22-6a	607	1075	−6.4	0.1	0.82	11.3	39.58	8.9	0.35	0.17	35.47	0.14	0.06	96.8
PEM22-6b	"	"	"	0.2	4.50	4.6	77.92	5.8	0.27	0.12	0.14	0.23	0.09	93.9
PEM22-7	731	1150	−5.9	0.1	0.65	19.7	22.19	14.8	0.22	0.15	40.81	0.16	0.18	98.9
PEM22-8	1017	1075	−7.1	0.2	1.54	13.5	39.33	11.0	0.26	0.26	29.63	0.19	0.18	96.1
PEM22-9	517	1125	−6.4	0.1	0.50	17.6	26.37	12.4	0.31	0.11	41.05	0.10	0.14	98.7
PEM22-10	1572	1120	−5.7	0.2	0.52	13.8	29.17	13.3	0.26	0.25	39.06	0.04	0.39	96.9
PEM22-12	2082	1050	−3.8	0.1	0.67	7.4	65.41	14.4	0.33	0.15	5.05	–	0.48	94.0
PEM22-13	2102	1075	−4.9	0.2	0.99	9.0	62.21	11.7	0.26	0.22	8.51	0.05	0.82	94.0

Phase diagram, phase compositions, and modes for basaltic andesite

The phase diagram generated from our water saturated experiments on the basaltic andesite composition is shown in Fig. 4. Note that it has similar properties as the andesite diagram in that plagioclase crystallization is suppressed by increased melt water content and that there appears to be a reaction relationship between hornblende and the other Fe-Mg phases (note the augite/olivine out line). Hornblende also appears to be stable to a slightly higher temperature than in the andesite (1000 °C vs 975 °C respectively).

The basaltic andesites of the WMVB have widely varying phenocryst assemblages and modal amounts despite similar bulk compositions (Fig. 6; Lange and Carmichael 1990; Carmichael et al. 1996). These phenocryst suites match experimental assemblages, proportions, and compositions, and show that the basaltic andesites had preeruptive dissolved water contents from below 2.0 to > 5.5 wt% (Fig. 4). A considerable range in water content can be represented by a single phenocryst assemblage (Figs. 4 and 7); for example, the "olivine-only" assemblage ranges in water content from ~2 to 6 wt%, while the range for olivine + plagioclase + augite is more restricted but still large (~2–5 wt%). Also shown on this diagram is the stability field for the hornblende lamprophyre (Mas-405; Carmichael et al. 1996). Although not well constrained by our experiments, this assemblage of hornblende + augite + olivine + plagioclase has its upper temperature limited by the stability of hornblende at 1000 °C. Its minimum pressure/water content is also limited by this hydrous phase to be > 1.5 kbar or ~ 4.5 wt% H_2O. However the upper bound on the water content for this assemblage is unconstrained by our experiments and could be greater than 6 wt%, depending on the behavior of the plagioclase stability field at higher pressures.

Phase compositions for the basaltic andesites

The compositions of the experimental phases match very closely the phenocryst compositions found in the lavas, suggesting that the conditions of the experiments are relevant to the conditions of crystal growth for the magmas. For example, the olivine and pyroxene com-

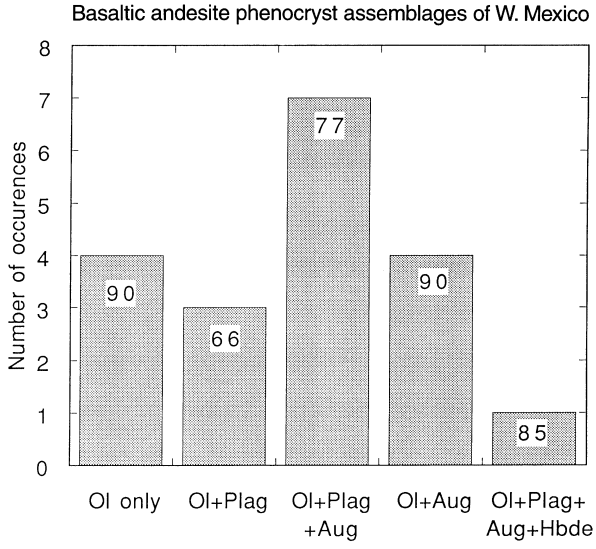

Fig. 6 Histogram of the phase assemblages and their frequency for the basaltic andesite composition (data from Lange and Carmichael 1990; Carmichael et al. 1996). *Numbers within the bars* represent the average modal% groundmass for each assemblage

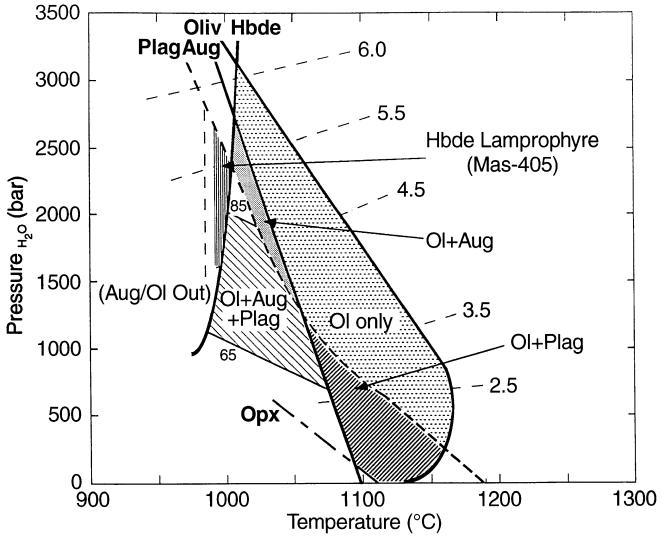

Fig. 7 Simplified phase diagram for the basaltic andesite showing the various phase assemblage fields. Water contours the same as in Figs. 3 and 4. Contours of % residual liquid at 65 and 85% in the olivine + augite + plagioclase field represent the range of observed % groundmass in the lavas

positions for the experiments (Table 5) are identical to those reported for the lavas with similar phenocryst phases (Lange and Carmichael 1990), indicating that the oxygen fugacity of the experiments is similar to the values at which the magmas came to equilibrium.

The normal compositional zoning found in the plagioclase phenocrysts in the basaltic andesites is about 10 mol% An ($An_{65–75}$) (Lange and Carmichael 1990). These compositions agree very well with the experimental feldspars from runs that reproduce the particular assemblage. Because of the strong dependence of plagioclase composition on the water content in the liquid (Housh and Luhr 1991), this observation suggests, in conjunction with the modal data discussed below, that the magmas are well represented by the hydrous conditions at which the experiments were run. For example, the feldspar phenocryst core compositions for the most frequent assemblage of olivine + plagioclase + augite range from An_{63} to An_{74} (Lange and Carmichael 1990), consistent with the range of feldspar compositions from experiments within the relevant phase field ($An_{63–81}$; Fig. 4).

Phase modes for the basaltic andesite assemblages

In general, the experimental phase abundances reproduce those found in the lavas with comparable phenocryst suites. For example, 3 of the 5 lavas containing only olivine have less than ~5% crystals (Lange and Carmichael 1990). The modal percentage of olivine has been contoured in Fig. 4 in the "olivine-only" field, and it can be seen that the 5% contour is very near the upper temperature stability for either augite or plagioclase and that the majority of the "olivine-only" field contains less than 5% crystals. The remaining two samples have slightly larger modal% olivine (6–7%) and are easily reconciled because of their higher concentration of MgO compared to the other samples. Again, this observation supports the hydrous nature of these lavas, as dry experiments could not reproduce both the phase assemblage of "olivine-only" and the correct proportion of crystals to liquid (i.e., plagioclase would always be present in anhydrous experiments).

The results of the experiments also agree so well with the other phenocryst modal abundances, that it is possible to use the modes of the lavas to constrain their equilibrium conditions and water content. For example, the assemblage olivine + augite + plagioclase shows a range in nature of 65 to 85% groundmass. This range is represented in Figs. 8A and B, which are plots of modal abundance of phases versus temperature at 1 and 2 kbar

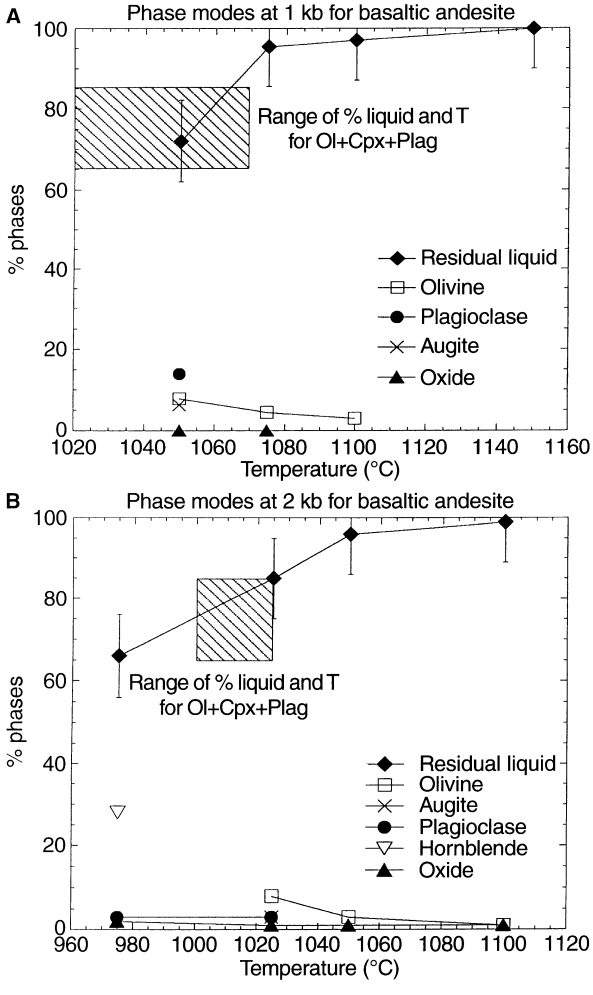

Fig. 8 A Phase modes as a function of temperature at 1 kilobar for the basaltic andesite. The *lined box* represents the range of % groundmass measured in lavas with the olivine + augite + plagioclase assemblage, as well as the temperature range for which the assemblage is stable at 1 kilobar. *Error bars* on liquid estimated from largest calculated residual. **B** Phase modes as a function of temperature at 2 kbar Symbols as above. *Lined box* represents range of % groundmass in the lavas, as well as temperature range for assemblage at 2 kilobars

respectively. Note that the amount of residual liquid in the experiments increases with pressure, and that the range observed in the lavas for the assemblage olivine + plagioclase + augite is approximately bracketed between 1–2 kbar, and 1025–1050 °C. This is shown in Fig. 7 by contours of approximate residual liquid percentages (65% and 85%) in the olivine + augite + plagioclase field. Another supporting observation, as was pointed out before, is that the feldspar compositions in the lavas mirror that of the experiments. Taken together, these lines of evidence show that these magmas grew phenocrysts at or near water saturated conditions with a water content between 3 and 5 wt%.

A similar analysis of modes was not possible for the olivine + plagioclase, hornblende lamprophyre, or the olivine + augite assemblages as only one experiment reproduced the first assemblage and the latter two were not reproduced at all. The low modal abundance of the groundmass for the olivine + plagioclase assemblage however (Fig. 6), is consistent with the relatively lower water contents (<3.5 wt% H_2O) predicted by the phase diagram. The olivine + augite assemblage is also consistent in that the phase diagram predicts significant water contents between ~4–5.5 wt%, and the average modal groundmass observed for this assemblage is also high at 90%.

Comparison to other Mexican basaltic andesites

In contrast to the basaltic andesites of western Mexico, lavas of similar composition found in the MGVF of central Mexico (Fig. 2) have phenocryst assemblages typical of low-H_2O, higher pressure conditions (Hasenaka and Carmichael 1987). A few of the basaltic andesites from the MGVF have hornblende as a phenocryst phase, but the majority consist of plagioclase, olivine, ± augite, ± orthopyroxene, which is defined on Fig. 4 as a region with low water content (<2 wt%). Hasenaka and Carmichael (1987) have speculated that the phenocryst equilibration conditions for the Mg-rich MGVF lavas are near 8 kilobars and undersaturated with 1–2 wt% H_2O, which is consistent with our estimated water concentrations of lavas at water saturated conditions of less than 500 bars; however our experiments do not allow the effects of pressure to be separated from P_{H_2O}.

A similar degassing history for the andesites and basaltic andesites of W. Mexico

With the similarity in bulk and trace element compositions for the andesites and basaltic andesites of western Mexico (Lange and Carmichael 1990; Carmichael et al. 1996), it is difficult to appeal to either crystal fractionation or different partial melting processes to explain the various phenocryst assemblages that are observed for each composition. The most simple and elegant explanation is that the different assemblages were generated as a consequence of the decompressional degassing and re-equilibration at different P-T conditions of initially hydrous parent magmas, similar to either the spessartite (andesite composition) or the hornblende lamprophyre (basaltic andesite composition). This hypothesis is supported for andesitic magma by the presence of plagioclase phenocryst cores in the Colima lavas that are more calcic (An_{65-85}) than the feldspars found in our experimental products at the relevant conditions (An_{63}). In fact, the calcic cores for Colima match the feldspar composition produced at ~2500 bars and 6.5 wt% H_2O (Fig. 3), consistent with the conclusion that the parent magma for Colima had similar water contents to that of the spessartite before ascent and storage (reequilibration) at depths equivalent to 750–1750 bars where the water concentration was reduced to saturation at those pressures (3–5 wt%).

For basaltic andesite magmas, the relations in Fig. 7 show that simple degassing of an initially hydrous parent magma (>5.5 wt% H_2O and ~1075 °C) could explain all of the observed phase assemblages, including the hornblende lamprophyre. In contrast to the andesites, the basaltic andesites do show some slight compositional variability however, indicating that fractionation or some other process may also play a role in the development of the different lava compositions. Lange and Carmichael (1990) noted that this compositional variation was best explained by fractionation of an assemblage of 1.6% olivine, 11.4% augite, and 4.4% chromite (sum $r^2 = 0.6$). Due to the relative paucity of augite phenocrysts in the lavas, they appealed to a two-stage crystallization history with augite fractionating at high pressure in conjunction with fractionation of olivine at low pressure without augite. Given the geometry of the phase fields this fractionation history is somewhat problematic as augite is never a liquidus phase and is stabilized with decreasing pressure, not destabilized as required by Lange and Carmichael (1990). Another possibility not previously considered is that hornblende was a fractionating phase. We have modeled the same two lavas (Mas-45 and Mas-7) as Lange and Carmichael (1990) did, using the program XLFRAC (Nicholls and Stormer 1978) and hornblende, augite, olivine, and chromite as possible fractionating phases. Interestingly, the best-fit assemblage (sum $r^2 = 0.27$) is 20.9% hornblende, 2.4% augite, and 1.3% chromite. While our experiments never produced a phase field of hornblende + augite (chromite is ubiquitous in our runs), the augite phase boundary is very near to crossing the olivine boundary at 3 kbar, so presumably the assemblage hornblende + augite would then be stable at ~3500 bars (~6 wt% H_2O) and greater (Figs. 4 and 7). The modes of augite and hornblende in the 3 kbar region (~5 and 25% respectively) are also consistent with that of the best-fit fractionating assemblage. This higher pressure fractionation assemblage, including hornblende, not only explains the compositional variation observed in the basaltic andesites, but is consistent with and supports the idea that the various phenocryst as-

semblages were generated by simple degassing and re-equilibration of an initially hydrous parent magma.

Petrogenetic link between the andesites and basaltic andesites of western Mexico

Given that the andesites and basaltic andesites both seem to have similar degassing histories and originated from parent magmas containing >5.5 wt% water, the question arises as to the possibility of the two compositions being genetically linked. Early attempts at modeling crystal fractionation from the basaltic andesite to the andesite (Mas-7 to Mas-12 respectively) were initially conducted with only the Fe-Mg phases common to the basaltic andesite at high pressures, and produced extremely high residuals (sum $r^2 > 4.0$). With the realization that plagioclase becomes more important in the evolved compositions, it was added as a potential fractionating phase. The results from these calculations showed that the best-fit assemblage (sum $r^2 = 0.74$) is 14.4% hornblende, 12.8% plagioclase (An_{75}), and 2.6% oxide. While not conclusive, these calculations suggest that it is possible that the andesites and basaltic andesites both come from a parent magma of similar major element composition and high (>6 wt%) water content. The differences in composition and phase assemblages are then explained by high pressure fractionation of varying degrees followed by degassing and re-equilibration at shallower levels in the crust.

Conclusions

High pressure (to 3 kilobars), hydrous ($P_{H_2O} = P_{total}$) melting experiments were conducted on a basaltic andesite and andesite to constrain the equilibration conditions of the phenocryst assemblages common to lavas of the western Mexican volcanic belt. Use of a rapid quench technique allowed precise measurement of residual liquid compositions in the run products, which in turn allowed the estimation of dissolved water contents using the empirical water solubility model of Moore et al. (1998), as well as accurate estimates of the modes of the various phases.

The experimental results and calculated water contents for the andesite composition indicate that the Colima andesite lavas last resided between 750 and 1500 bars and 950–975 °C, and the residual liquid contained 3.5–4.5 wt% H_2O. These results are in agreement with the conditions estimated by Luhr and Carmichael (1980) using pyroxene thermometry and feldspar/liquid equilibria (Luhr 1998). As the compositions of all the Fe-Mg phases in the experiments and the lavas are similar, we conclude that the oxygen fugacity of the experiments ($\sim$NNO + 2) is similar to that of the magma. The Mascota spessartite assemblage formed at a similar temperature to the Colima andesite, but equilibrated above 2500 bars pressure and had greater than $\sim$5.5 wt% H_2O in the liquid. A slightly higher Mg/Fe ratio in the spessartite hornblendes relative to the Colima andesite indicates that the spessartite equilibrated at a higher oxygen fugacity, which is confirmed by comparisons of the whole rock ferric/ferrous ratios measured by Carmichael et al. (1996). Results for the basaltic andesite composition show that a wide range in dissolved water content (2–5.5 wt%) is necessary to generate the various phase assemblages observed, thereby verifying the postulate of Lange and Carmichael (1990) that significant but variable amounts of water occur in these subduction-related lavas. This observation is in contrast to basaltic andesites from the MGVF that require <2 wt% H_2O.

Due to the similarity in composition between the various lava types and the results of the phase equilibria experiments we conclude that all of the phenocryst assemblages observed for each composition can be explained by degassing and reequilibration of a hydrous parent magma containing greater than 6 wt% water. Calculation of crystal fractionation processes using high pressure phases including hornblende can explain the variation in composition within the basaltic andesites, as well as suggest the possibility that the andesites were generated from a similar parent magma as the basaltic andesites.

Acknowledgements The support of NSF grant EAR 94-18105 was essential to this research. Cogent reviews by Tom Sisson and an anonymous reviewer greatly improved the presentation and refined the analysis of the data.

References

Baker DR, Eggler DH (1987) Compositions of anhydrous and hydrous melts coexisting with plagioclase, augite, and olivine or low-Ca pyroxene from 1 atm to 8 kbar: application to the Aleutian volcanic center of Atka. Am Mineral 72: 12–28

Carmichael ISE, Lange RA, Luhr JF (1996) Quaternary minettes and associated volcanic rocks of Mascota, western Mexico: a consequence of plate extension above a subduction modified mantle wedge. Contrib Mineral Petrol 124: 302–333

Eggler DH (1972) Water-saturated and undersaturated melting relations in a paricutin andesite and an estimate of water content in the natural magma. Contrib Mineral Petrol 34: 261–271

Eggler DH, Burnham CW (1973) Crystallization and fractionation trends in the system andesite-H_2O-CO_2-O_2 at pressures to 10 kbar. Geol Soc Am Bull 84: 2517–2532

Ewart A (1982) The mineralogy and petrology of Tertiary–Recent orogenic volcanic rocks, with special reference to the andesitic-basaltic compositional range. In: Thorpe RS (ed) Orogenic andesites and related rocks. Wiley, New York, pp 25–95

Gill JB (1981) Orogenic andesites and plate tectonics. Springer-Verlag; Berlin Heidelberg, New York.

Green DH, Ringwood AE (1968) Genesis of the calc-alkaline igneous rock suite. Contrib Mineral Petrol 18: 105–162

Hasenaka T, Carmichael ISE (1987) The cinder cones of Michoacan-Guanajuato, Central Mexico: petrology and chemistry. J Petrol 28: 241–269

Holloway JR, Burnham CW (1972) Melting relations of basalt with equilibrium water pressure less than total pressure. J Petrol 13: 1–29

Holloway JR, Dixon JE, Pawley AR (1992) An internally heated, rapid-quench, high pressure vessel. Am Mineral 77: 643–646

Housh TB, Luhr JF (1991) Plagioclase-melt equilibria in hydrous systems. Am Mineral 76: 477–492

Huebner JS, Sato M (1970) The oxygen fugacity-temperature relationships of manganese oxide and nickel oxide buffers. Am Mineral 55: 934–952

Kress, VC, Carmichael ISE (1991) The compressibility of silicate liquids containing Fe_2O_3 and the effect of composition, temperature, oxygen fugacity and pressure on their redox states. Contrib Mineral Petrol 108: 82–92

Lange RA, Carmichael ISE (1990) Hydrous basaltic andesites associated with minette and related lavas in western Mexico. J Petrol 31: 1225–1259

Luhr JF (1990) Experimental phase relations of water- and sulfur-saturated arc magmas and the 1982 eruptions of El Chichon volcano. J Petrol 31: 1071–1114

Luhr JF (1992) Slab-derived fluids and partial melting in subduction zones: insights from two contrasting Mexican volcanoes (Colima and Ceboruco). J Volcanol Geothermal Res 54: 1–18

Luhr JF, Carmichael ISE (1980) The Colima volcanic complex, Mexico. I. Post caldera andesites from Volcan Colima. Contrib Mineral Petrol 71: 343–372

Merzbacher C, Eggler DH (1984) A magmatic geohygrometer: application to Mount St. Helens and other dacitic magmas. Geology 12: 587–590

Moore GM, Vennemann T, Carmichael ISE (1998) An empirical model for the solubility of water in magmas to 3 kilobars, Am Mineral, in press

Moore G, Righter K, Carmichael ISE (1995) The effect of dissolved water on the oxidation state of iron in natural silicate liquids. Contrib Mineral Petrol 120: 170–179

Nicholls J, Stormer JC (1978) XLFRAC: a program for the interactive testing of magmatic differentiation models. Comput Geosci 4: 143–159

Osborn EF (1959) Role of oxygen pressure in the crystallization and differentiation of basaltic magma. Am J Sci 257: 609–647

Pownceby MI, O'Neil HSC (1994) Thermodynamic data from redox reactions at high temperatures. III. Activity-composition relations in Ni-Pd alloys from EMF measurements at 850–1250 K, and calibration of the NiO + Ni-Pd assemblage as a redox sensor. Contrib Mineral Petrol 116: 327–339

Rutherford MJ, Devine JD (1988) The May 18, 1980, eruption of Mount St. Helens 3. Stability and chemistry of amphibole in the magma chamber. J Geophys Res 93: 11949–11959

Rutherford MJ, Hill PM (1993) Magma ascent rates from amphibole breakdown: an experimental study applied to the 1980–1986 Mount St. Helens eruptions. J Geophys Res 98: 19667–19685

Rutherford MJ, Sigurdsson H, Carey S, Davis A (1985) The May 18, 1980, eruption of Mount St. Helens melt composition and experimental phase equilibria. J Geophys Res 90: 2929–2947

Sisson TW, Grove TL (1993a) Experimental investigations of the role of H_2O in calc-alkaline differentiation and subduction zone magmatism. Contrib Mineral Petrol 113: 143–166

Sisson TW, Grove TL (1993b) Temperatures and H_2O contents of low-MgO high alumina basalts. Contrib Mineral Petrol 113: 167–184

Sisson TW, Layne GD (1993) H_2O in basalt and basaltic andesite glass inclusions from four subduction-related volcanoes. Earth Planet Sci Lett 117: 619–635

Taylor JR, Wall VJ, Pownceby MI (1992) The calibration and application of accurate redox sensors. Am Mineral 77: 284–295

Wallace P, Carmichael ISE (1992) Alkaline and calc-alkaline lavas near Los Volcanes, Jalisco, Mexico: geochemical diversity and its significance in volcanic arcs. Contrib Mineral Petrol 111: 423–439

Wallace P, Carmichael ISE, Righter K, Becker TA (1992) Volcanism and tectonism in western Mexico: a contrast of style and substance. Geology 20: 625–628